Scaling Laws in the Ductile Fracture of Metallic Crystals

M. I. Baskes
Bagley College of Engineering,
Mississippi State University,
Mississippi, MS 39762;
Jacobs School of Engineering,
University of California, San Diego,
La Jolla, CA 92093;
Los Alamos National Laboratory,
Los Alamos, NM 87545

M. Ortiz
Division of Engineering and Applied Science,
California Institute of Technology,
Pasadena, CA 91125

We explore whether the continuum scaling behavior of the fracture energy of metals extends down to the atomistic level. We use an embedded atom method (EAM) model of Ni, thus bypassing the need to model strain-gradient plasticity at the continuum level. The calculations are performed with a number of different 3D periodic size cells using standard molecular dynamics (MD) techniques. A void nucleus of a single vacancy is placed in each cell and the cell is then expanded through repeated NVT MD increments. For each displacement, we then determine which cell size has the lowest energy. The optimal cell size and energy bear a power-law relation to the opening displacement that is consistent with continuum estimates based on strain-gradient plasticity (Fokoua et al., 2014, "Optimal Scaling in Solids Undergoing Ductile Fracture by Void Sheet Formation," Arch. Ration. Mech. Anal. (in press); Fokoua et al., 2014, "Optimal Scaling Laws for Ductile Fracture Derived From Strain-Gradient Microplasticity," J. Mech. Phys. Solids, ***62****, pp. 295–311). The persistence of power-law scaling of the fracture energy down to the atomistic level is remarkable.* [DOI: 10.1115/1.4030329]

1 Introduction

Ductile fracture is the process whereby a material separates across a failure surface through mechanisms, such as void nucleation, growth, and coalescence, that entail large amounts of plastic work. Owing to its engineering importance, ductile fracture has been the focus of extensive study and one of the main driving forces in the development of nonlinear fracture mechanics (cf., e.g., Refs. [1] and [2] for reviews). Unlike brittle fracture, where the behavior of the material is ostensibly elastic up to fracture, in ductile fracture the plastic dissipation attendant to void growth and coalescence accounts for a significant or even dominant part of the energy budget. Such extensive plastic deformation notwithstanding, failure ultimately takes place by separation across a plane or surface and entails a well-characterized amount of energy per unit area, or specific fracture energy, to operate. In consequence, typical measured specific fracture energies for ductile fracture are much larger than those of brittle solids and exhibit a characteristic temperature dependence that includes a brittle-to-ductile transition at a critical temperature.

A number of micromechanical and computational models have been put forth (cf., e.g., Refs. [3–18]), including consideration of nonlocal effects (cf., e.g., Refs. [19–22]) and scaling [23] that account for the observational evidence and relate macroscopic properties to material structure and behavior at the microscale. These works are overwhelmingly computational in nature. By way of sharp contrast, there is a paucity of analytical approaches capable of establishing explicit connections between micromechanical properties and ductile fracture, and specifically scaling laws thereof.

Recently, Fokoua, Conti, and Ortiz (FCO) [24,25] have performed a continuum optimal-scaling analysis of ductile fracture in metals and have shown that ductile fracture in metals can be explained as the outcome of two competing effects: their relatively low plastic-hardening rates, which enables geometric instabilities such as the necking and strain localization, and strain-gradient plasticity. Specifically, FCO derive an upper bound on the fracture energy by considering a separation mechanism in the form of a void sheet. The fracture energy upper bound exhibits well-defined power-law scaling with separation and the characteristic length of strain-gradient plasticity. In particular, the exponents in the scaling relation follow explicitly from the hardening exponent of the material. FCO then proceed to show mathematically that the void-sheet upper bound is indeed optimal in the sense of optimal scaling, i.e., they prove a lower bound of the fracture energy that scales identically to the upper bound. In this manner, the scaling exponents are shown to be intrinsic to the material and not just an artifact of a suboptimal upper bound construction.

The essence of the FCO void-sheet construction may be understood as follows. Consider a slab of material of dimensions $L \times L \times H$, where H is the thickness of the slab (Fig. 1). The slab deforms under periodic boundary conditions on its sides and under prescribed normal displacements $\pm\delta$. Localize the deformations to a band of thickness a within the slab and subdivide this band into L^2/a^2 cubes of size a. Assume that the outside of the band moves rigidly, so that each cube deforms under periodic boundary conditions on its sides with its other two faces displaced through $\pm\delta$. If the material is nearly incompressible, for large δ a void is expected to nucleate from the center of the cube. The total deformation-theoretical energy of the voided slab scales as [1,2]

$$E^{\text{tot}}_{\text{slab}} = \frac{L^2}{a^2} E^{\text{tot}}_{\text{cube}} = KL^2 \left[\left(\frac{\delta}{a} \right)^n a + \ell \frac{\delta}{a} \right] \tag{1}$$

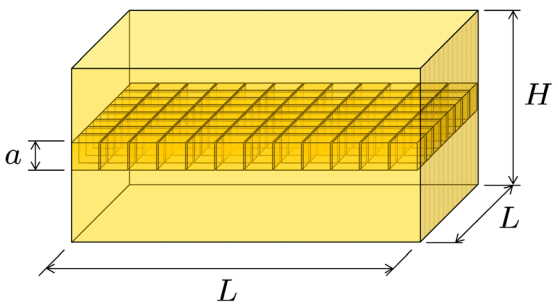

Fig. 1 Periodic unit cell of infinite slab of thickness *H* deforming under prescribed opening displacements δ on its surface. The deformations localize to a band of thickness *a*, which further subdivides into $\sim L^2/a^2$ cubes of size *a*. A void nucleates from the center of every cube and then expands to accommodate the volume increase of the band.

Contributed by the Applied Mechanics Division of ASME for publication in the JOURNAL OF APPLIED MECHANICS. Manuscript received January 1, 2015; final manuscript received March 29, 2015; published online June 3, 2015. Assoc. Editor: A. Amine Benzerga.

where K is a material constant, $0 < n < 1$ is the hardening exponent of the metal, and $\ell > 0$ is the characteristic length of strain-gradient plasticity. The first term in Eq. (1) arises as a result of local plastic hardening as the void expands, whereas the second term is the contribution of strain-gradient plasticity. Minimizing $E^{\text{tot}}_{\text{slab}}$ with respect to a, we obtain

$$a = \delta^{\alpha}\ell^{1-\alpha} \tag{2}$$

with

$$\alpha = \frac{1-n}{2-n} \tag{3}$$

We note that the optimal cube size (2) increases as a power of the prescribed opening displacement δ, a form of coarse-graining that is in keeping with observation. Inserting these optimal values into the slab energy gives

$$E^{\text{tot}}_{\text{slab}} = KL^2\ell^{\alpha}\delta^{1-\alpha} \tag{4}$$

independently of the slab thickness H.

We note from Eq. (4) that the energy of the slab exhibits power-law scaling with respect to the in-plane size L of the slab, the opening displacement δ, and the intrinsic length ℓ of strain-gradient plasticity. Specifically, the energy scales as L^2 and is independent of the thickness H of the slab. This type of scaling is characteristic of fracture processes, in which the deformation is concentrated on a fracture surface and the energy scales with the area of that surface. In particular, the specific energy per unit area $E^{\text{tot}}_{\text{slab}}/L^2$ is well defined as a material property. As a corollary, fractal modes of fracture, characterized by energy scaling intermediate between area and volume scaling, are ruled out under the assumptions of the analysis.

2 Evidence of Scaling at the Atomistic Level

In the present work, we carry out a similar analysis at the atomistic level. In so doing, we explore whether the continuum scaling behavior extends down to the atomistic level, thus bypassing the need to model strain-gradient plasticity at the continuum level. We use an EAM model of Ni [26,27] that reproduces the elastic and surface properties of Ni reasonably well. The EAM surface energy is ~20% less than experiment and the stacking fault energy is ~30% less than experiment. The elastic constants are within 1% of experiment.

The calculations are performed with a number of different size cells ($\sim 300 - 10^5$ atoms per cell), each of which consists of $2 \le N \le 14$ multiples in each direction of a small orthorhombic single crystal unit cell of size ~ 7.5Å$\times$ ~ 8.6Å$\times$ ~ 6Å and directions $x = [1\bar{1}0], y = [11\bar{2}], z = [111]$, which we take as the basic cell. We choose these cell directions to facilitate dislocation activity.

All calculations are performed with 3D periodic cells using standard MD techniques, including a Nose–Hoover thermostat [28,29] and a 2 fs time step. All calculations are carried out at an average temperature of 300 K and zero pressure. Each simulation is run for a time of 10 ps and average properties are calculated over the last 5 ps of the simulation. The equilibrium lattice constant is obtained by running an NpT simulation of a perfect cell. This lattice constant is used for all subsequent calculations in the x- and y-directions.

A void nucleus of a single vacancy is placed in each cell and the average energy of the cell is calculated using NVT MD. The cell is then expanded by a small amount and the NVT MD is repeated. This process is repeated until total times of ~2 ns are reached. This procedure results in strain rates of $\sim 3\text{ns}^{-1}$ for the small cells to 1ns^{-1} for the larger cells. We realize that these are large strain rates compared to most laboratory experiments and fully expect that the results will be strain rate dependent. Investigation of the strain rate dependence is beyond the scope of the present research.

In Fig. 2, the results of the calculations just described are presented. We subtract the energy of a perfect cell at 300 K from the cell energy to yield an energy that is representative of the deformation. This stored energy includes contributions from the elastic, plastic, and surface energies. We scale this energy by the surface energy of perfect fracture, so that a scaled energy of unity represents that of perfect cleavage. This scaled energy represents the energy of Eq. (4) divided by L^2. For all cell sizes, we observe the following three features: (1) an initial almost linear increase in energy with displacement with a slope decreasing with increasing cell size; (2) a critical displacement, which increases with cell size, where the energy decreases rapidly with displacement and then slowly increases to a plateau; and (3) plateau energies which increase with increasing cell size and are always greater than unity.

We now interpolate these energy curves to obtain the scaled energy at specific displacements. For each displacement, we determine which cell size has the lowest energy. In Fig. 3, we see the number of periods, N, increases with displacement. The full curve in the figure is a power law as in Eq. (2) with $\alpha = 0.3$.

In addition, in Fig. 4 we see that the lowest energy follows a similar power law with the power $1 - \alpha$, as expected from Eq. (4).

Note that from Eq. (3) we can calculate n, the strain hardening exponent. For the value of $\alpha = 0.3$ found above, $n = 0.57$. This value is higher than the literature value of 0.39 [30], but considering the scale of the simulations, the high strain rate, and possible anisotropy effects, the agreement is not unreasonable.

We can explain the shape of the energy curve by examining the microstructural aspects of the simulations. In Fig. 5, we reproduce the energy curve of Fig. 2 for $N = 6$. Looking at any other size cell would result in similar analysis.

We quantify the atom environment using the common neighbor analysis (CNA) [31] implemented in OVITO [32]. The first dislocation activity occurs at a very small scaled displacement of ~ 0.2, as indicated by the circle in Fig. 5. At the peak energy, the results of the CNA (Fig. 6(*a*)) show significant dislocation activity manifested by the presence of stacking faults and dislocation cores. After the energy drop (Fig. 6(*b*)), the number of stacking faults and dislocation cores is reduced significantly, while the voids show significant growth. Finally, (Fig. 6(*c*)) after the cell has fractured there are essentially no dislocations remaining in the cell. We speculate that, if we continued the calculations to much larger cell sizes, the dislocation density after fracture and the plateau energy would continue to increase due to the fact that the dislocations would not be able to annihilate at free surfaces and would naturally form loops and locks.

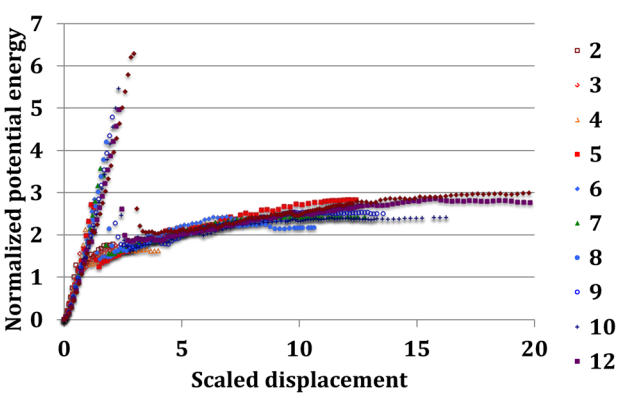

Fig. 2 Energy relative to the unstrained cell normalized by the (111) surface area versus cell displacement scaled by the *z*-direction cell size of the basic cell (~ 6Å) for various cell sizes denoted by the number of basic cells in each direction

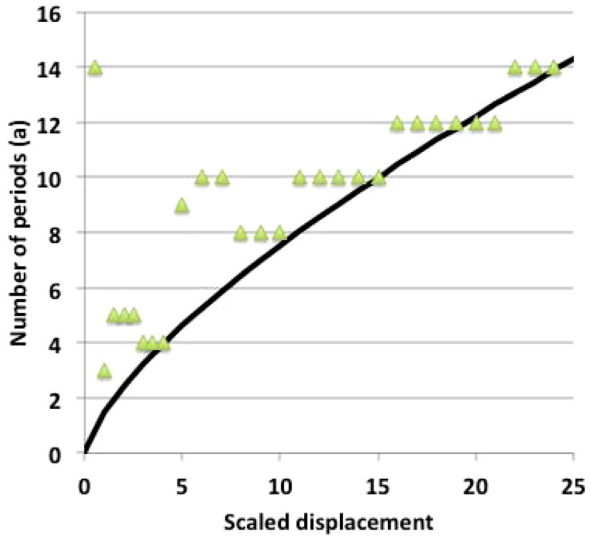

Fig. 3 Number of periods in the cell with the lowest energy as a function of the scaled displacement

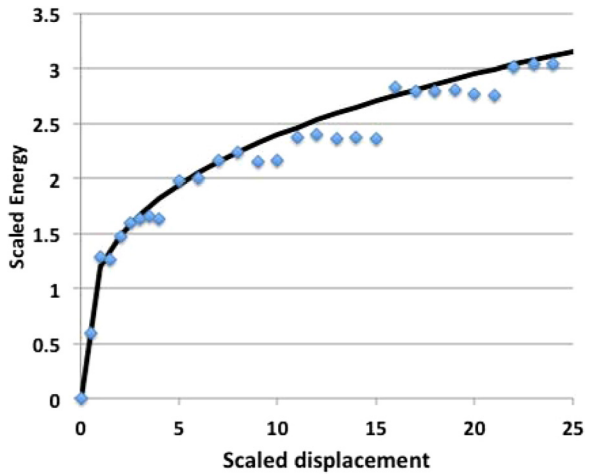

Fig. 4 Lowest energy as a function of the scaled displacement

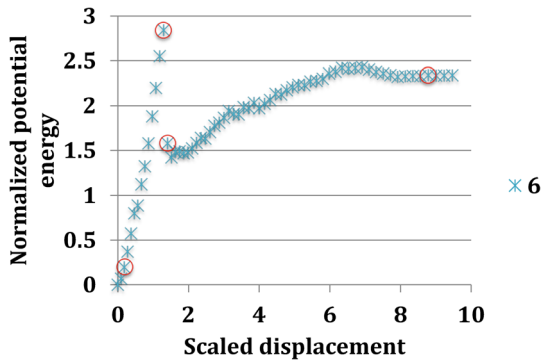

Fig. 5 Energy relative to the unstrained cell normalized by the (111) surface area versus cell displacement scaled by the *z*-direction cell size of the basic cell ($\sim$ 6Å) for $N = 6$. CNA was performed at the points indicated by circles.

We also have analyzed the void growth and fracture of this cell using the surface mesh software implemented in OVITO. Results are shown in Fig. 7, where we present a $2 \times 2 \times 2$ replication of our cell to show the voids and fracture surface more clearly. It is clear that there has been significant void growth after the energy

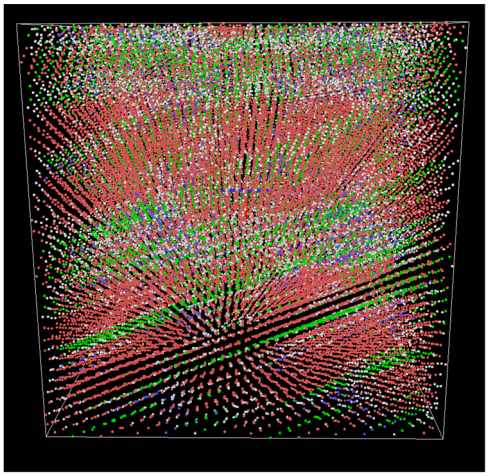

(a)

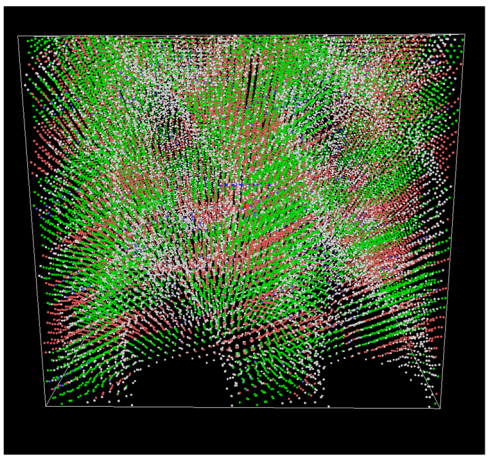

(b)

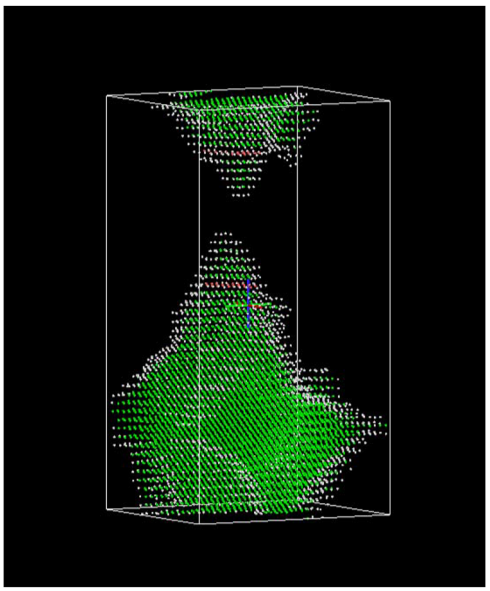

(c)

Fig. 6 CNA at (*a*) the peak energy, (*b*) after the energy drop, and (*c*) after fracture. Fcc atoms are denoted as green, hcp (stacking fault) as red, bcc as blue, and unknown (dislocation core, vacancy, and free surface) as white.

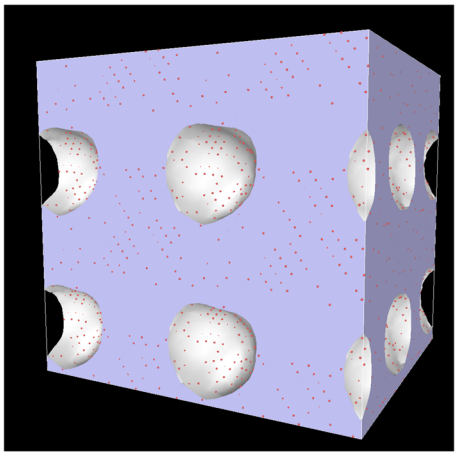

(a)

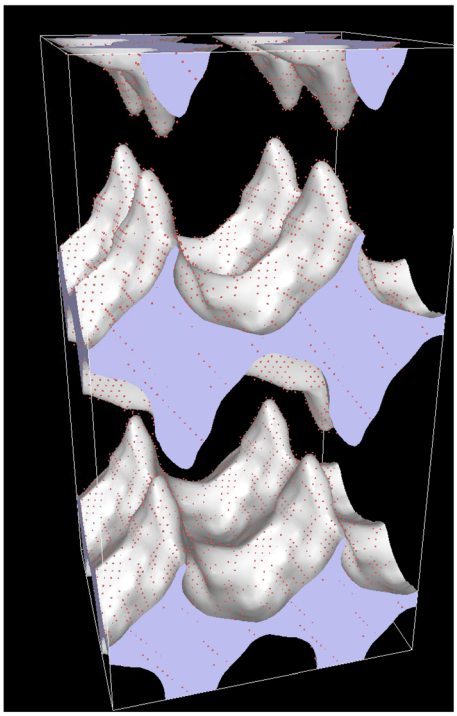

(b)

Fig. 7 Surfaces at (*a*) after the energy drop and (*b*) after fracture as indicated by the circles in Fig. 5

drop as indicated in Fig. 7(*a*). Figure 7(*b*) shows the rough fracture surface, which has resulted in a scaled plateau energy significantly greater than unity.

3 Conclusions

It is encouraging that the scaling of the cell size and energy are nearly consistent and that the value of α implies a hardening exponent of nickel $n < 1$. Indeed, the persistence of power-law scaling of the fracture energy down to the atomistic level is remarkable.

The atomistic and continuum models of plasticity and void evolution have similar behavior. By examining the microstructural evolution in our simulations it is clear that the initial increase in energy is due to a dislocation density increase under deformation. Void growth causes a sharp decrease in energy followed by an increase in energy and then fracture under increasing deformation. The void density decrease results in a lower stored energy than would occur with constant void density, as predicted by the FCO analysis.

In closing, we emphasize that the scaling behavior under consideration is asymptotic for large opening displacement δ and may there well be other regimes of interest, e.g., during nucleation, that are best studied using other tools of analysis. We also note that the FCO analysis suggests that the scaling exponents are independent of the geometry of the unit cell, indicative of the arrangement of void nucleation sites, though the scaling constants are not. The determination of optimal-scaling constants is beyond the scope of the FCO analysis and remains an open problem.

Acknowledgment

MO gratefully acknowledges the support of the U.S. National Science Foundation through the Partnership for International Research and Education (PIRE) on Science at the Triple Point Between Mathematics, Mechanics, and Materials Science, Award No. 0967140.

References

[1] Hutchison, J. W., 1979, *A Course on Nonlinear Fracture Mechanics*, Department of Solid Mechanics, TU Denmark, Lyngby, Denmark.
[2] Kanninen, M. F., and Popelar, C. H., 1985, "Advanced Fracture Mechanics," *Oxford Engineering Science Series*, Oxford University Press, New York.
[3] Ritchie, R. O., Knott, J. F., and Rice, J. R., 1973, "Relationship Between Critical Tensile Stress and Fracture Toughness in Mild-Steel," J. Mech. Phys. Solids, **21**(6), pp. 395–410.
[4] Rice, J. R., and Thomson, R., 1974, "Ductile Versus Brittle Behavior of Crystals," Philos. Mag., **29**(1), pp. 73–97.
[5] Needleman, A., 1982, "Continuum Analyses of Localization and Ductile Fracture," J. Metals, **35**(12), p. A70.
[6] Tvergaard, V., 1982, "Ductile Fracture by Cavity Nucleation Between Larger Voids," J. Mech. Phys. Solids, **30**(4), pp. 265–286.
[7] Becker, R., Needleman, A., Richmond, O., and Tvergaard, V., 1988, "Void Growth and Failure in Notched Bars," J. Mech. Phys. Solids, **36**(3), pp. 317–351.
[8] Koplik, J., and Needleman, A., 1988, "Void Growth and Coalescence in Porous Plastic Solids," Int. J. Solids Struct., **24**(8), pp. 835–853.
[9] Becker, R., Needleman, A., Suresh, S., Tvergaard, V., and Vasudevan, A. K., 1989, "An Analysis of Ductile Failure by Grain-Boundary Void Growth," Acta Metall., **37**(1), pp. 99–120.
[10] Tvergaard, V., 1990, "Material Failure by Void Growth to Coalescence," Adv. Appl. Mech., **27**, pp. 83–151.
[11] Needleman, A., and Tvergaard, V., 1991, "A Numerical Study of Void Distribution Effects on Dynamic, Ductile Crack-Growth," Eng. Fract. Mech., **38**(2–3), pp. 157–173.
[12] Tvergaard, V., 1992, "A Numerical-Analysis of 3D Localization Failure by a Void-Sheet Mechanism," Eng. Fract. Mech., **41**(6), pp. 787–803.
[13] Tvergaard, V., and Hutchinson, J. W., 2002, "Two Mechanisms of Ductile Fracture: Void by Void Growth Versus Multiple Void Interaction," Int. J. Solids Struct., **39**(13–14), pp. 3581–3597.
[14] Pardoen, T., and Hutchinson, J. W., 2003, "Micromechanics-Based Model for Trends in Toughness of Ductile Metals," Acta Mater., **51**(1), pp. 133–148.
[15] Tvergaard, V., and Niordson, C., 2004, "Nonlocal Plasticity Effects on Interaction of Different Size Voids," Int. J. Plast., **20**(1), pp. 107–120.
[16] Tvergaard, V., 2007, "Discrete Modelling of Ductile Crack Growth by Void Growth to Coalescence," Int. J. Fract., **148**(1), pp. 1–12.
[17] Xue, Z., Pontin, M. G., Zok, F. W., and Hutchinson, J. W., 2010, "Calibration Procedures for a Computational Model of Ductile Fracture," Eng. Fract. Mech., **77**(3), pp. 492–509.
[18] Nielsen, K. L., and Tvergaard, V., 2011, "Failure by Void Coalescence in Metallic Materials Containing Primary and Secondary Voids Subject to Intense Shearing," Int. J. Solids Struct., **48**(9), pp. 1255–1267.
[19] Tvergaard, V., and Needleman, A., 1997, "Nonlocal Effects on Localization in a Void-Sheet," Int. J. Solids Struct., **34**(18), pp. 2221–2238.
[20] Borg, U., Niordson, C. F., Fleck, N. A., and Tvergaard, V., 2006, "A Viscoplastic Strain Gradient Analysis of Materials With Voids or Inclusions," Int. J. Solids Struct., **43**(16), pp. 4906–4916.
[21] Niordson, C. F., 2008, "Void Growth to Coalescence in a Non-Local Material," Eur. J. Mech. A-Solids, **27**(2), pp. 222–233.
[22] Nielsen, K. L., Niordson, C. F., and Hutchinson, J. W., 2012, "Strain Gradient Effects on Steady State Crack Growth in Rate-Sensitive Materials," Eng. Fract. Mech., **96**, pp. 61–71.
[23] Needleman, A., Tvergaard, V., and Bouchaud, E., 2012, "Prediction of Ductile Fracture Surface Roughness Scaling," ASME J. Appl. Mech., **79**(3), p. 031015.
[24] Fokoua, L., Conti, S., and Ortiz, M., 2014, "Optimal Scaling in Solids Undergoing Ductile Fracture by Void Sheet Formation," Arch. Ration. Mech. Anal., **212**(1), pp. 331–357.

[25] Fokoua, L., Conti, S., and Ortiz, M., 2014, "Optimal Scaling Laws for Ductile Fracture Derived From Strain-Gradient Microplasticity," J. Mech. Phys. Solids, **62**, pp. 295–311.
[26] Angelo, J. E., Moody, N. R., and Baskes, M. I., 1995, "Trapping of Hydrogen to Lattice Defects in Nickel," Modell. Simul. Mater. Sci. Eng., **3**(3), pp. 289–307.
[27] Baskes, M. I., Sha, X., Angelo, J. E., and Moody, N. R., 1997, "Trapping of Hydrogen to Lattice Defects in Nickel," Modell. Simul. Mater. Sci. Eng., **5**(6), pp. 651–652.
[28] Nosé, S., 1984, "A Unified Formulation of the Constant Temperature Molecular Dynamics Methods," J. Chem. Phys., **81**(1), pp. 511–519.
[29] Hoover, W. G., 1985, "Dynamics: Equilibrium Phase-Space Distributions," Phys. Rev. A, **31**(3), p. 1695.
[30] ASM, 2002, *Atlas of Stress–Strain Curves*, ed., ASM International, Materials Park, OH.
[31] Faken, D., and Jónsson, H., 1994, "Systematic Analysis of Local Atomic Structure Combined With 3D Computer Graphics," Comput. Mater. Sci., **2**(2), pp. 279–286.
[32] Stukowski, A., and Albe, K., 2010, "Extracting Dislocations and Non-Dislocation Crystal Defects From Atomistic Simulation Data," Modell. Simul. Mater. Sci. Eng., **18**(8), p. 085001.